Title

Poly zinc finger protein ZFP14 suppresses lymphomagenesis and abnormal inflammatory response via the HOXA gene cluster

Journal

Biochimica et Biophysica Acta (BBA) - Molecular Basis of Disease, 1869(1)

ISSN

0925-4439

Authors

Mohibi, Shakur

Chen, Mingyi

Chen, Xinbin

et al.

Publication Date

2023

DOI

10.1016/j.bbadis.2022.166587

Peer reviewed

HHS Public Access

Author manuscript

Biochim Biophys Acta Mol Basis Dis. Author manuscript; available in PMC 2024 March 02.

Published in final edited form as:

Biochim Biophys Acta Mol Basis Dis. 2023 January 01; 1869(1): 166587. doi:10.1016/j.bbadis.2022.166587.

Poly zinc finger protein ZFP14 suppresses lymphomagenesis and abnormal inflammatory response *via* the *HOXA* gene cluster

Shakur Mohibi[a,*], **Mingyi Chen**[b], **Xinbin Chen**[a,*], **Jin Zhang**[a,*]

[a]Comparative Oncology Laboratory, Schools of Veterinary Medicine and Medicine, University of California, Davis, CA, United States of America

[b]Department of Pathology, University of Texas Southwestern Medical Center, Dallas, TX, United States of America

Abstract

Poly zinc finger proteins (ZFP) that contain a KRAB (Krüppel-associated box) domain represent the largest class of transcription factors in higher organisms, but their roles in development and pathogenesis are largely undefined. ZFP14 (also known as ZNF531) contains thirteen zinc fingers and is highly conserved across species. Notably, we found that *ZFP14* is frequently down-regulated in a multitude of human cancers, which correlates with poor prognosis of patients. Since ZFP14 has never been characterized, we generated a *Zfp14*-deficient mouse model to investigate the role of ZFP14 in development and pathogenesis. We showed that the mice deficient in *Zfp14* had a short lifespan and were prone to diffuse large B-cell lymphoma (DLBCL), hyperplasia in multiple organs, systemic chronic inflammation, liver steatosis, and pancreatitis. Additionally, several pro-inflammatory cytokines, including IL-1β, IL18, and TNFα, were highly expressed in inflamed $Zfp14^{-/-}$ mice spleens, livers, kidneys and lungs. To determine the underlying mechanism, RNA-seq analysis was performed and showed that the loss of ZFP14 led to increased expression of inflammatory and tumor-promoting genes. Out of the various tumor-promoting genes upregulated by ZFP14 loss, the *HOXA* gene cluster, which is known to promote lymphomagenesis and conserved between mouse and human, is consistently induced by loss of ZFP14. Moreover, we showed that the *HOXA* gene expression was inversely correlated with that of *ZFP14* in human cancer patients and higher *HOXA1* expression was correlated with poor patient prognosis. Together, we postulate that ZFP14 suppresses lymphomagenesis and abnormal inflammatory response by maintaining proper expression of the *HOXA* gene cluster.

*Corresponding authors.: smohibi@ucdavis.edu (S. Mohibi), xbchen@ucdavis.edu (X. Chen), jinzhang@ucdavis.edu (J. Zhang).

Declaration of competing interest

The authors declare no competing interests.

CRediT authorship contribution statement

Shakur Mohibi: Conceptualization, Resources, Data curation, Investigation, Methodology, Writing – original draft, Writing – review & editing. **Mingyi Chen:** Formal analysis. **Xinbin Chen:** Conceptualization, Resources, Supervision, Funding acquisition, Methodology, Writing – original draft, Writing – review & editing. **Jin Zhang:** Resources, Data curation, Supervision, Methodology, Writing – original draft, Writing – review & editing.

Appendix A. Supplementary data

Supplementary data to this article can be found online at https://doi.org/10.1016/j.bbadis.2022.166587.

Keywords

ZFP14; Diffuse large B-cell lymphoma; Inflammation; HOXA gene cluster

1. Introduction

KRAB-ZFP proteins consist of a KRAB (Krüppel-associated box) domain followed by multiple zinc fingers and form the largest group of transcription factors in mammals [1,2]. KRAB-ZFPs are largely considered as DNA-binding transcriptional repressors and can activate transcription as well as bind to RNA and proteins to execute their key functions [2–4]. KRAB-ZFPs generally contain a KRAB domain at its N-terminus, followed by 10 or more tandem repeats of zinc fingers. The KRAB domain generally facilitates the recruitment of repressive complexes *via* its corepressor KRAB associated protein 1 (KAP1) [5] whereas the zinc finger domain aids in the recognition of specific nucleotides in DNA/RNA or specific amino-acids in proteins [3,6]. In the human genome, there are approximately 423 KRAB-ZFPs with only 103 KRAB-ZFP genes conserved across mammals [7], suggesting a functional diversity and lineage specificity of this special family.

Although several KRAB-ZFPs have been associated with the development and silencing of retro elements, the biological functions of most KRAB-ZFPs remain unknown and even less is known about their role in physiology and various diseases, including cancer. For the KRAB-ZFPs linked to various cancers, most of them are predicted to function as tumor suppressor genes, but some are known to be overexpressed in cancers and might act as oncogenes [8].

To explore the role of KRAB-ZFPs in cancer, we examined the expression profile of KRAB-ZFPs in various types of human cancers by analyzing the TCGA database with the focus on the conserved KRAB-ZFPs. We found that several KRAB-ZFPs with unknown functions, including ZFP14, were frequently altered in human cancers. ZFP14 (also known as ZNF531), which was originally identified from human adult and fetal brain cDNA libraries [9], is conserved across mammals and ubiquitously expressed in many tissues. Human ZFP14 contains 534 amino acids and shares 88 % sequence similarity with mouse Zfp14. Notably, the signature residues in all 13 zinc fingers are completely conserved between mouse and human ZFP14. Sequence alignment indicates that ZFP14 contains an N-terminal KRAB domain followed by 13 zinc fingers towards its C-terminus. Based on these functional domains, ZFP14 is predicted to regulate transcription by binding to sequence-specific DNA. However, the biological or physiological functions of ZFP14 have never been analyzed.

TCGA database showed that the low expression of ZFP14 correlates with poor prognosis in human cancer patients, suggesting a role of ZFP14 in tumor suppression. Thus, we took an initiative to explore the biology of ZFP14 with a focus on its role in tumorigenesis. To analyze the role of ZFP14 *in vivo*, we generated a *Zfp14*-deficient mouse model and found that loss of ZFP14 led to a shortened lifespan and increased incidence of spontaneous tumors, chronic inflammation, and liver steatosis. To understand the mechanism underlying multifaceted functions of ZFP14, RNA-seq was performed and showed that the

loss of ZFP14 led to increased expression of inflammatory and tumor-promoting genes, in particular, the HOXA gene cluster, which is known to promote lymphomagenesis and conserved between mouse and human [10–12]. Moreover, we showed that the HOXA gene expression was inversely correlated with that of ZFP14 in human cancer patients. Together, we postulate that ZFP14 suppresses lymphomagenesis and abnormal inflammatory response by maintaining a proper expression level of the HOXA gene cluster.

2. Materials and methods

2.1. Cell culture, cell line generation and reagents

The human cancer cell line HCT116 was obtained from ATCC and used within 2 months of thawing or below passage 20. The human DLBCL cell lines, Pfeiffer and SUDHL6, were a gift from Dr. Hongwu Chen at University of California, Davis. HCT116 cells were cultured in Dulbecco's modified Eagle's medium (DMEM) (Invitrogen) supplemented with 10 % fetal bovine serum (FBS) (Hyclone, Logan, UT). Pfeiffer and SUDHL6 cells were cultured in RPMI-1640 medium (Invitrogen) supplemented with 10 % FBS (Hyclone, Logan, UT). Generation of *ZFP14-KO* HCT116 cell lines was achieved by pSpCas9(BB)-2A-Puro vector expressing guide RNAs. The cells were selected with puromycin, and individual clones picked, genotyped, sequenced, and confirmed by PCR. The primers used for genotyping are listed in Supplementary Table S4.

2.2. RNA isolation and RT-PCR

Total RNA was harvested and isolated using TRIzol reagent (Invitrogen). 2 μg total RNA was used to synthesize cDNA using RevertAid First Strand cDNA Synthesis kit according to the manufacturer's protocol (ThermoFisher Scientific™). The levels of various transcripts were measured by semiquantitative and/or quantitative PCR with primers listed in Supplementary Table S5.

2.3. sgRNAs to generate knockout cell lines

To generate *ZFP14-KO* cells, two single-guide RNA (sgRNA) expression vectors pSpCas9(BB)-2A-Puro-sgZFP14–1 and pSpCas9(BB)-2A-Puro-sgZFP14–2 were used to remove exon 3 and create frame shift deletion. The generation of sgRNA expression vector was performed as described previously [13]. The oligonucleotides used for cloning sgZFP14–1 are sense, 5′-CAC CGG ATA GCA TGC AAA CAG CAT T-3′, and antisense, 5′-AAA CAA TGC TGT TTG CAT GCT ATC C-3′; for sgZfp14–2 are sense, 5′-CAC CGC TTT CTC TGC TGT CAA TTT C-3′, and antisense, 5′-AAA CGA AAT TGA CAG CAG AGA AAG C-3′.

2.4. Mice

The use of animals and the study protocols were approved by the University of California at Davis Institutional Animal Care and Use Committee. *Zfp14*$^{+/-}$ mice were generated by the Mouse Biology Program at the University of California, Davis (Davis, CA, USA). The primers used to genotype the *Zfp14*-WT or *Zfp14*-KO allele are listed in Supplementary Table S4.

2.5. Mouse embryonic fibroblast (MEF) isolation

MEFs were isolated from 12.5 to 13.5 days post-coitum (pc) mouse embryos, as described previously [14]. To generate WT, *Zfp14*$^{+/-}$ and *Zfp14*$^{-/-}$ MEFs, *Zfp14*$^{+/-}$ mice were interbred. The MEFs were cultured in DMEM supplemented with 10 % FBS (Hyclone Laboratories, Erie, PA, USA), 55 μM β-mercaptoethanol and 1× non-essential amino acids solution (Cellgro, Manassas, VA, USA).

2.6. Histological analysis

Mouse tissues were fixed in 10 % neutral buffered formalin, processed, and embedded in paraffin blocks. Tissue blocks were sectioned (6 μm) and stained with H&E.

2.7 . RNA-seq analysis

Total RNA was harvested from two isogenic controls (#24 and #41) and two *ZFP14*-KO (#10 and #25) HCT116 cells using TRIzol reagent (Invitrogen). 1 % agarose gels were used to monitor RNA degradation. NanoPhotometer spectrophotometer (IMPLEN, CA, USA) was used to measure RNA purity, whereas the RNA Nano 6000 Assay Kit of the Bioanalyzer 2100 system (Agilent Technologies, CA, USA) was used to assess RNA integrity and quantitation. RNA sample preparation was performed by using 1 μg of RNA per sample. NEBNext UltraTM RNA Library Prep Kit from Illumina (NEB, USA) was used to generate sequencing libraries following manufacturer's recommendations and index codes were added to attribute sequences to each sample. Briefly, poly-T oligo-attached magnetic beads were used to purify mRNA from the total RNA. The mRNA was fragmented in NEBNext First Strand Synthesis Reaction Buffer containing divalent cations under elevated temperature. Following this, random hexamer primers and M-MuLV Reverse Transcriptase (RNase H-) was used to synthesize first strand cDNA. Subsequently, DNA polymerase I and RNase H were used to perform second strand cDNA synthesis. Overhangs remaining after second strand synthesis were converted into blunt ends by exonuclease/polymerase activities. 3′ ends of DNA fragments were adenylated and ligated with NEBNext Adaptor with hairpin loop structure to prepare for hybridization. cDNA fragments of preferentially 150– 200 bp in length were selected by purifying the library fragments with AMPure XP system (Beckman Coulter, Beverly, USA). Then 3 μl USER Enzyme (NEB, USA) at 37 °C for 15 min followed by 5 min at 95 °C before PCR. Then PCR was performed with Phusion High-Fidelity DNA polymerase, Universal PCR primers and Index (X) Primer. Finally, PCR products were purified (AMPure XP system) and library quality was assessed on the Agilent Bioanalyzer 2100 system.

2.8. RNA-seq data analysis

2.8.1. Quality control—Raw data (raw reads) of FASTQ format were initially processed through fastp. In this step, clean data (clean reads) were obtained by removing reads containing adapter and poly-N sequences and reads with low quality from raw data. At the same time, Q20, Q30 and GC content of the clean data were calculated. All the downstream analyses were based on the clean data with high quality.

2.8.2. Mapping to reference genome—Reference genome hg19 and gene model annotation files were downloaded from genome website browser (NCBI/UCSC/Ensembl) directly. Paired-end clean reads were aligned to the hg19 reference genome using the Spliced Transcripts Alignment to a Reference (STAR) software, which is based on a previously undescribed RNA-seq alignment algorithm that uses sequential maximum mappable seed search in uncompressed suffix arrays followed by seed clustering and stitching procedure. STAR exhibits better alignment precision and sensitivity than other RNA-seq aligners for both experimental and simulated data.

2.8.3. Quantification—FeatureCounts was used to count the read numbers mapped of each gene. And then RPKM of each gene was calculated based on the length of the gene and reads count mapped to this gene. RPKM, Reads Per Kilo-base of exon model per Million mapped reads, considers the effect of sequencing depth and gene length for the reads count at the same time.

2.8.4. Differential expression analysis—Prior to differential gene expression analysis for each sequenced library, the read counts were adjusted by Trimmed Mean of M-values (TMM) through one scaling normalized factor. Differential expression analysis of two conditions was performed using the edgeR R package. The *P* values were adjusted using the Benjamini and Hochberg methods. Corrected *p*-value of 0.005 and $\left|\log_2^{(\text{Fold Change})}\right|$ of 1 were set as the threshold for significantly differential expression.

2.8.5. GO enrichment analysis—GO is the abbreviation of Gene Ontology (http://www.geneontology.org/), which is a major bioinformatics classification system to unify the presentation of gene properties across all species. GO enrichment analysis of differentially expressed genes was implemented by the clusterProfiler R package. GO terms with corrected *P* value <0.05 were considered significantly enriched by differential expressed genes.

2.9. Statistical analysis

Mice survival analysis was performed by Kaplan–Meier survival analysis using the log rank test. Data are presented as means ± standard error of the mean (SEM). The *p* values for qRT-PCRs were calculated using the two-tailed Student's *t*-tests, and $p < 0.05$ was considered statistically significant. For each experimental data point, $n = 3$. Excel (Microsoft, Redmond, WA) was used for statistical analyses.

3. Results

3.1. Low levels of ZFP14 correlate with poor prognosis in human cancer patients

To identify the cancer relevant KRAB-ZFPs that could predict human patient prognosis, we examined the expression of several KRAB-ZFPs from the TCGA database using Xena browser. Many of the KRAB-ZFPs we examined were from recently reported publications shown to have aberrant expression in cancers [8,15]. Notably, out of the about 20 cancer-relevant KRAB-ZFPs examined, lower expression of ZFP14 significantly correlated with poor overall survival, poor disease-free survival and poor progression-free survival in human

cancer patients from TCGA pan-cancer database (Figs. 1A–C). Moreover, lower ZFP14 expression significantly correlated with poor patient survival in specific cancer types (Figs. 1D–J). Thus, we focused on ZFP14 to determine its role in tumorigenesis.

Human ZFP14 (ZNF531) contains an N-terminal KRAB domain followed by a linker region and 13 zinc fingers (Fig. 1K). Mouse Zfp14 is 88 % similar to human ZFP14 and consists of the same domains as human ZFP14 (Fig. 1K and Supplementary Fig. S1). Importantly, variable residues at positions −1, +2, +3 and +6 of each zinc finger that decide the substrate identity are identical between human and mouse ZFP14 (Fig. 1K), indicating conservation of their function across species.

3.2. Zfp14$^{-/-}$ and Zfp14$^{+/-}$ mice have a shorter lifespan and are prone to spontaneous tumors

As lower ZFP14 levels in human cancer patients correlate with poor patient survival, we reasoned that the *Zfp14*-KO mice should be susceptible to spontaneous tumor formation. Thus, a *Zfp14*-deficient mouse model was generated using traditional embryonic stem cell targeting strategy and confirmed by genotyping (Supplementary Fig. S2A and B).

To examine the biological functions of Zfp14 *in vivo*, a cohort of *Zfp14*$^{+/-}$ and *Zfp14*$^{-/-}$ mice was generated and monitored for long-term survival, predisposition to tumors and other pathological abnormalities. We would like to note that to reduce the numbers of mice used, WT mice were adapted from previous studies [16,17]. Nevertheless, these WT mice had the same C57BL/6 genetic background as *Zfp14*-deficient mice and were maintained in the same facility. We found that the median lifespan for *Zfp14*$^{+/-}$ (n = 34; 86.9 weeks) and *Zfp14*$^{-/-}$ (n = 19; 80 weeks) mice were significantly shorter than that for WT mice (n = 56; 117 weeks) (Fig. 2A; Supplementary Tables S1–S3). However, there was no significant difference in median lifespan between *Zfp14*$^{+/-}$ and *Zfp14*$^{-/-}$ mice (Fig. 2A). Moreover, we found that when compared to WT mice, both *Zfp14*$^{+/-}$ and *Zfp14*$^{-/-}$ mice were prone to spontaneous tumors (Fig. 2B; Supplementary Tables S1–S3). The tumor penetrance of 43.3 % in *Zfp14*$^{+/-}$ mice was significantly higher than that in WT mice (21.6 %) (Fig. 2B, p-value = 0.047 by Fisher's exact test). Similarly, the tumor penetrance in *Zfp14*$^{-/-}$ (47.1 %) was higher than in WT mice, but it was not statistically significant (Fig. 2B, p-value = 0.061 by Fisher's exact test). Notably, while both WT and *Zfp14*-deficient mice were prone to lymphomas, we found that the incidence of diffuse large B cell lymphoma (DBLCL) was markedly increased in both *Zfp14*$^{+/-}$ and *Zfp14*$^{-/-}$ mice as compared to that in WT mice (WT *vs.* *Zfp14*$^{+/-}$: p = 0.0113; WT *vs.* *Zfp14*$^{-/-}$: p = 0.0041 by Fisher's exact test) (Fig. 2C, Supplementary Tables S1–S3). Indeed, 11 out of 30 *Zfp14*$^{+/-}$ mice and 8 out of 17 *Zfp14*$^{-/-}$ mice, whereas only 6 out of 51 WT mice, developed DLBCL, suggesting that *Zfp14*-deficiency promotes B-cell lymphomagenesis.

3.3. Zfp14-deficient mice are susceptible to inflammation in multiple organs

In addition to increased tumor formation in *Zfp14*-deficient mice, we examined the major organs for other potential abnormalities by performing histological analysis. Histopathological analyses indicated that the mice deficient in Zfp14 developed chronic inflammation in multiple organs including liver, lung, and salivary gland (Fig. 3A). In fact,

90 % of *Zfp14*$^{+/-}$ and 94 % *Zfp14*$^{-/-}$ mice were found to develop chronic inflammation in >3 organs and 46.7 % of *Zfp14*$^{+/-}$ and 82.3 % of *Zfp14*$^{-/-}$ mice developed inflammation in >4 organs (Fig. 3B, Supplementary Tables S2–S3). By contrast, not a single WT mouse developed chronic inflammation in >3 or 4 organs (Fig. 3B, Supplementary Table S1). Additionally, *Zfp14*$^{-/-}$ mice exhibited a marked increase in the percentage of mice with inflammation in >4 organs when compared to *Zfp14*$^{+/-}$ (Fig. 3B).

When comparing inflammation in a single organ, *Zfp14*-deficiency enhanced the susceptibility of mice to pancreatitis, as well as liver, lung, kidney, and salivary gland inflammation (Figs. 3C–D; Supplementary Fig. S3A–D). Moreover, we observed substantially increased levels of various inflammatory cytokine mRNAs in spleen, liver, kidney and lung of *Zfp14*-deficient mice compared to WT mice (Fig. 3E–H). As DLBCLs associated with increased inflammation have been identified as a separate class of tumors by World Health Organization and are associated with more advanced stage and poor patient survival in humans [18,19], the above findings suggest that the *Zfp14*-deficient mice develop aggressive DLBCL.

3.4. Zfp14-deficient mice develop liver steatosis and are prone to hyperplasia in several organs

In addition to inflammation, we also looked for other abnormalities in *Zfp14*-deficient mice organs. Interestingly, we showed that both *Zfp14*$^{+/-}$ and *Zfp14*$^{-/-}$ mice developed liver steatosis at a significantly higher rate compared to WT mice (Fig. 4A–B; Supplementary Tables S1–S3), indicating aberrant lipid metabolism in *Zfp14*-deficient mice.

Additionally, compared to WT, both *Zfp14*$^{+/-}$ and *Zfp14*$^{-/-}$ mice had significantly higher occurrence of hyperplasia in spleen, thymus, skin and lymph nodes (Figs. 4C–G; Supplementary Tables S1–S3), emphasizing their susceptibility to increased tumor formation. Taken together, *Zfp14*-deficient mice are susceptible to increased liver steatosis and hyperplasia in various organs in addition to their susceptibility to DLBCL formation and inflammation.

3.5. ZFP14-KO leads to increased expression of inflammatory and tumor-promoting genes

Although increased inflammation could result in increased tumorigenesis observed in the *Zfp14*-deficient mice [20,21], we generated *ZFP14-KO* HCT116 human colorectal cancer cells using CRISPR-Cas9 and performed RNA-seq analysis to determine the genes and pathways regulated by ZFP14 that might be involved in tumorigenesis (Fig. 5A–B). Notably, we found that ZFP14 differentially regulated several pathways linked to the abnormalities we observed in *Zfp14*-deficient mice, such as hyperplasia, pancreatitis, and dermatitis (Fig. 5B). Moreover, we found that the *ZFP14*-deficiency leads to up-regulation of multiple inflammatory cytokines as well as their receptors (Fig. 5B–C), corroborating with increased inflammation seen in the *Zfp14*-deficient mice.

Furthermore, we observed increased expression of several tumor-promoting genes upon *ZFP14* deletion. These genes included genes from the *HOXA* cluster, the L-type amino acid transporter *SLC7A8*, the G-protein coupled receptor *ADGRF1*, secretory leukocyte

peptidase inhibitor *SLPI* and the transcription factor *RUNX2* (Fig. 5D). Based on its predicted function as a transcriptional repressor, most of the genes altered upon *ZFP14* deletion were upregulated (Fig. 5C–D). Interestingly, *ZFP14* deletion led to the increased expression of all the *HOXA* cluster genes including the non-coding RNA *HOTAIRM1* transcribed from the *HOXA* cluster (Fig. 5D), indicating involvement of ZFP14 in repressing the entire *HOXA* gene cluster.

3.6. ZFP14 modulates tumorigenesis by regulating the expression of the HOXA gene cluster in humans and mice

Next, we confirmed the increased expression of the tumor-promoting genes obtained from the RNA-seq analysis, by qRT-PCR, in HCT116 *ZFP14*-KO cells (Fig. 6A). We were able to confirm the increased expression of most of the tumor promoting genes, except *RUNX2* (Fig. 6A), showing the reproducibility of the RNA-seq data. Interestingly, all three *HOXA* cluster genes confirmed by qRT-PCR showed significant increase upon *ZFP14*-KO (Fig. 6A), reaffirming the regulation of the *HOXA* cluster by ZFP14.

As ZFP14 function in cancer appeared to be similar in mouse and humans, we next examined if the regulation of some of the tumor-promoting genes by ZFP14 in human cells is also conserved in mouse cells. For this, we performed qRT-PCR in WT and $Zfp14^{-/-}$ MEFs and showed that the regulation of the entire *HoxA* gene cluster by ZFP14 appeared to be conserved in mice (Fig. 6B). However, the huge increase in expression of *SLPI* and *SLC7A8* observed in *ZFP14*-KO human cells was not observed in *Zfp14*-KO MEFs (Fig. 6B). Previous studies showed that HOXA cluster is frequently up-regulated in human B-cell lymphomas and promotes leukemia in animal models [22–24]. Thus, we further corroborated the *HOXA* cluster regulation by ZFP14 in human DLBCL cell lines, Pfeiffer and SUDHL6. As these are suspension cell lines, we knocked down *ZFP14* in these cell lines using electroporation. As seen in Fig. 6C, we observed a robust decrease of *ZFP14* mRNA in *ZFP14*-KD samples. Importantly, we saw a significant increase of the *HOXA1* mRNA levels in these cells (Fig. 6D), re-affirming the negative regulation of the *HOXA* genes by ZFP14. Next, we analyzed *HoxA* gene expression in the DLBCL present in the spleen of $Zfp14^{-/-}$ mice as well as in the WT and $Zfp14^{-/-}$ mice liver tissues. As seen in Fig. 6E, we observed increased expression of *HoxA1* and *HoxA9* mRNAs in spleen from $Zfp14^{-/-}$ mice that had DLBCL, suggesting the increased expression of the *HoxA* genes could be responsible for promoting DLBCL in the *Zfp14*-KO mice. Moreover, we also showed increased *HoxA* gene expression in the liver tissues of $Zfp14^{-/-}$ mice as compared to the WT mice (Fig. 6F).

Since ZFP14 is involved in repressing the *HOXA* cluster gene expression, we analyzed the TCGA pan cancer database and showed that *HOXA1* mRNA expression inversely correlated with that of *ZFP14* in cancer tissues (Fig. 6G). Moreover, we also showed that contrary to *ZFP14*, higher *HOXA1* expression correlated with poor patient prognosis in the pan cancer TCGA database (Figs. 1A and 6H) as well in specific tumor types (Fig. 1D, H, I and Supplementary Fig. S4A–C), underscoring the inverse correlation of *ZFP14* and *HOXA* gene expression in cancer. Taken together, ZFP14 appears to suppress tumorigenesis by repressing the expression of the *HOXA* gene cluster in human and mice.

4. Discussion

The KRAB-ZFPs consist of the largest family of transcriptional factors in higher organisms [1,2]. Although recent studies indicated that the expression of many KRAB-ZFPs is altered in several tumor types, the role of KRAB-ZFP in cancer remains ambiguous [8,15]. To expand our knowledge of KRAB-ZFPs in cancer, we carried out a study to determine physiological significance of ZFP14, a KRAB-ZFP with unknown function, by using multiple genetic and biomedical approaches. We showed that the lower expression of *ZFP14* correlates with poor prognosis in human cancer patients as well as in mice. Specifically, we found that *Zfp14*-deficient mice were prone to increased inflammation and developed aggressive DLBCL, which is in part mediated by its regulation of the *HOXA* gene cluster.

DLBCL is the most common form of non-Hodgkin's lymphoma in humans and accounts for about 49 % of the B-cell cancer worldwide [25,26]. Even with better treatment options available, approximately half of the patients with DLBCL show recurrence or have a poor outcome [25]. Recently, systemic immune-inflammation has emerged as a prognostic biomarker in DLBCL that can assist in separating high-risk patients [18,19]. Notably, patients with DLBCL that show higher systemic immune-inflammation have advanced disease and poor survival [18,19]. Not only DLBCL with increased inflammation are aggressive, but continuous chronic inflammation itself can act as a predisposition for tumor formation and metastasis [27]. As *Zfp14*-deficient mice are prone to multi-organ inflammation possibly due to elevated expression of pro-inflammatory cytokines, it is reasonable to assume that ZFP14 has an anti-inflammatory activity. Although acute inflammation is transient and beneficial to the organism, chronic inflammation elevates cancer risk in multiple organs, underscoring the function of the immune system in promoting tumorigenesis [21,28]. In line with this, we showed that several pro-inflammatory cytokines along with their receptors were up-regulated by loss of *ZFP14* in mouse tissues and human cells. Indeed, like ZFP14, ZNF300 and ZNF281 have been shown to regulate inflammation *in vitro* [29,30]; however, their roles in inflammation *in vivo* have yet to be explored. Nonetheless, these data suggest that ZFP14 may have a profound role in modulating inflammatory response, which might be responsible for the development of aggressive DLBCL in *Zfp14*-deficient mice. While the regulation of inflammation may be a direct consequence of *ZFP14* loss, increased *HOXA* gene expression resulting from *Zfp14* deletion may also contribute to cancer-promoting inflammation [10]. These findings, although intriguing, warrant further work.

The clusters of the *Hox* family of genes are evolutionarily conserved and encode for DNA-binding transcription factors that are essential for anteroposterior body axis patterning during early development and are frequently dysregulated in cancers [10–12]. Of the four *Hox* gene clusters, the overexpression of genes from the *HOXA* cluster not only can cause leukemia in animal models, but are also overexpressed in human cancers [22–24]. Likewise, identifying factors that can regulate the *HOX* gene expression in normal as well as cancer cells is an important area of research in cancer biology. Although an underlying mechanism is not elucidated here, it is possible that ZFP14 functions as a transcriptional repressor to modulate expression of the *HOXA* gene cluster since they are located closely and often regulated simultaneously [31]. Thus, further studies are needed to elucidate how ZFP14

modulates the *HOXA* gene cluster and its role in the development of B-cell lymphoma. Taken together, we conclude that the ZFP14-HOXA pathway plays an indispensable role in inflammation and cancer formation in mouse and humans.

Supplementary Material

Refer to Web version on PubMed Central for supplementary material.

Acknowledgements

We would like to thank members of the Chen-Zhang laboratory for suggestions and helpful discussions. This work is supported in part by National Institutes of Health grants [CA224433 and CA250338 to XC].

Data availability

All the data are available in the main text or the supplementary materials. The datasets used and/or analyzed during the current study are available from the corresponding author on reasonable request.

References

[1]. Ecco G, Imbeault M, Trono D, KRAB zinc finger proteins, Development 144 (15) (2017) 2719–2729. [PubMed: 28765213]

[2]. Emerson RO, Thomas JH, Adaptive evolution in zinc finger transcription factors, PLoS Genet. 5 (1) (2009).

[3]. Gamsjaeger R, Liew CK, Loughlin FE, Crossley M, Mackay JP, Sticky fingers: zinc-fingers as protein-recognition motifs, Trends Biochem. Sci. 32 (2007) 63–70. [PubMed: 17210253]

[4]. Cassandri M, Smirnov A, Novelli F, Pitolli C, Agostini M, Malewicz M, et al. , Zinc-finger proteins in health and disease, Cell Death Discov. 3 (2017).

[5]. Friedman JR, Fredericks WJ, Jensen DE, Speicher DW, Huang XP, Neilson EG, et al. , KAP-1, a novel corepressor for the highly conserved KRAB repression domain, Genes Dev. 10 (16) (1996) 2067–2078. [PubMed: 8769649]

[6]. Brown RS, Zinc finger proteins: getting a grip on RNA, Curr. Opin. Struct. Biol. 15 (1) (2005) 94–98. [PubMed: 15718139]

[7]. Huntley S, Baggott DM, Hamilton AT, Tran-Gyamfi M, Yang S, Kim J, et al. , A comprehensive catalog of human KRAB-associated zinc finger genes: insights into the evolutionary history of a large family of transcriptional repressors, Genome Res. 16 (5) (2006) 669–677. [PubMed: 16606702]

[8]. Sobocińska J, Molenda S, Machnik M, Oleksiewicz U, Krab-zfp transcriptional regulators acting as oncogenes and tumor suppressors: an overview, Int. J. Mol. Sci. 22 (4) (2021) 1–27.

[9]. Nagase T, Kikuno R, Nakayama M, Hirosawa M, Ohara O, Prediction of the coding sequences of unidentified human genes. XVIII. The complete sequences of 100 new cDNA clones from brain which code for large proteins in vitro, DNA Res. 7 (4) (2000) 273–281. [PubMed: 10997877]

[10]. Pai P, Sukumar S, HOX genes and the NF-κB pathway: a convergence of developmental biology, inflammation and cancer biology, Biochim. Biophys. Acta - Rev. Cancer 1874 (2) (2020), 188450. [PubMed: 33049277]

[11]. Argiropoulos B, Humphries RK, Hox genes in hematopoiesis and leukemogenesis, Oncogene 26 (47) (2007) 6766–6776. [PubMed: 17934484]

[12]. Brotto DB, Siena ÁDD, de Barros II, da C. e.S Carvalho S, Muys BR, Goedert L, et al. , Contributions of HOX genes to cancer hallmarks: enrichment pathway analysis and review, Tumor Biol. 42 (5) (2020) 1–16.

[13]. Ran FA, Hsu PD, Wright J, Agarwala V, Scott DA, Zhang F, Genome engineering using the CRISPR-Cas9 system, Nat. Protoc. [Internet] 24 (8) (2013 Oct) 2281, 10.1038/nprot.2013.143. Available from:.

[14]. Mohibi S, Zhang J, Chen M, Chen X, Mice deficient in the RNA-binding protein Zfp871 are prone to early death and steatohepatitis in part through the p53–Mdm2 axis, Mol. Cancer Res. 19 (10) (2021) 1751–1762. [PubMed: 34257081]

[15]. Machnik M, Cylwa R, Kiełczewski K, Biecek P, Liloglou T, Mackiewicz A, et al. , The expression signature of cancer-associated KRAB-ZNF factors identified in TCGA pan-cancer transcriptomic data, Mol. Oncol. 13 (4) (2019) 701–724. [PubMed: 30444046]

[16]. Zhang Y, Qian Y, Zhang J, Yan W, Jung YS, Chen M, et al. , Ferredoxin reductase is critical for p53-dependent tumor suppression via iron regulatory protein 2, Genes Dev. 31 (12) (2017) 1243–1256. [PubMed: 28747430]

[17]. Yang HJ, Zhang J, Yan W, Cho SJ, Lucchesi C, Chen M, et al. , Ninjurin 1 has two opposing functions in tumorigenesis in a p53-dependent manner, Proc. Natl. Acad. Sci. U. S. A. 114 (43) (2017) 11500–11505. [PubMed: 29073078]

[18]. Wang Z, Zhang J, Luo S, Zhao X, Prognostic significance of systemic immune-inflammation index in patients with diffuse large B-cell lymphoma, FrontOncol. (2021) 11.

[19]. Sun F, Zhu J, Lu S, Zhen Z, Wang J, Huang J, et al. , An inflammation-based cumulative prognostic score system in patients with diffuse large B cell lymphoma in rituximab era, BMC Cancer 18 (1) (2018).

[20]. Coussens LM, Werb Z, Inflammation and cancer, Nature 420 (2002) 860–867. [PubMed: 12490959]

[21]. Greten FR, Grivennikov SI, Inflammation and cancer: triggers, mechanisms, and consequences, Immunity 51 (2019) 27–41. [PubMed: 31315034]

[22]. Bach C, Buhl S, Mueller D, García-Cuéllar MP, Maethner E, Slany RK, Leukemogenic transformation by HOXA cluster genes, Blood 115 (14) (2010) 2910–2918. [PubMed: 20130239]

[23]. Breitinger C, Maethner E, Garcia-Cuellar MP, Slany RK, The homeodomain region controls the phenotype of HOX-induced murine leukemia, Blood 120 (19) (2012) 4018–4027. [PubMed: 22990017]

[24]. Chen SL, Qin ZY, Hu F, Wang Y, Dai YJ, Liang Y, The role of the hoxa gene family in acute myeloid leukemia, Genes (Basel) 10 (8) (2019).

[25]. Roschewski M, Staudt LM, Wilson WH, Diffuse large B-cell lymphoma - treatment approaches in the molecular era, Nat. Rev. Clin. Oncol. 11 (1) (2014) 12–23. [PubMed: 24217204]

[26]. Hunt KE, Reichard KK, Diffuse large B-cell lymphoma, Arch. Pathol. Lab. Med. 132 (2008) 118–124. [PubMed: 18181663]

[27]. Baecklund E, Smedby KE, Sutton LA, Askling J, Rosenquist R, Lymphoma development in patients with autoimmune and inflammatory disorders - What are the driving forces? Semin. Cancer Biol. 24 (2014) 61–70. [PubMed: 24333759]

[28]. Coussens LM, Werb Z, Inflammation and cancer, Available from, Nature [Internet] 420 (6917) (2002) 860–867, https://www.ncbi.nlm.nih.gov/pubmed/12490959. [PubMed: 12490959]

[29]. Wang T, Wang XG, Xu JH, Wu XP, Qiu HL, Yi H, et al. , Overexpression of the human ZNF300 gene enhances growth and metastasis of cancer cells through activating NF-kB pathway, J. Cell. Mol. Med. 16 (5) (2012) 1134–1145. [PubMed: 21777376]

[30]. Pierdomenico M, Palone F, Cesi V, Vitali R, Mancuso AB, Cucchiara S, et al. , Transcription factor ZNF281: a novel player in intestinal inflammation and fibrosis, Front. Immunol. (2018) 9.

[31]. Cao K, Collings CK, Marshall SA, Morgan MA, Rendleman EJ, Wang L, et al. , SET1A/COMPASS and shadow enhancers in the regulation of homeotic gene expression, Genes Dev. 31 (8) (2017) 787–801. [PubMed: 28487406]

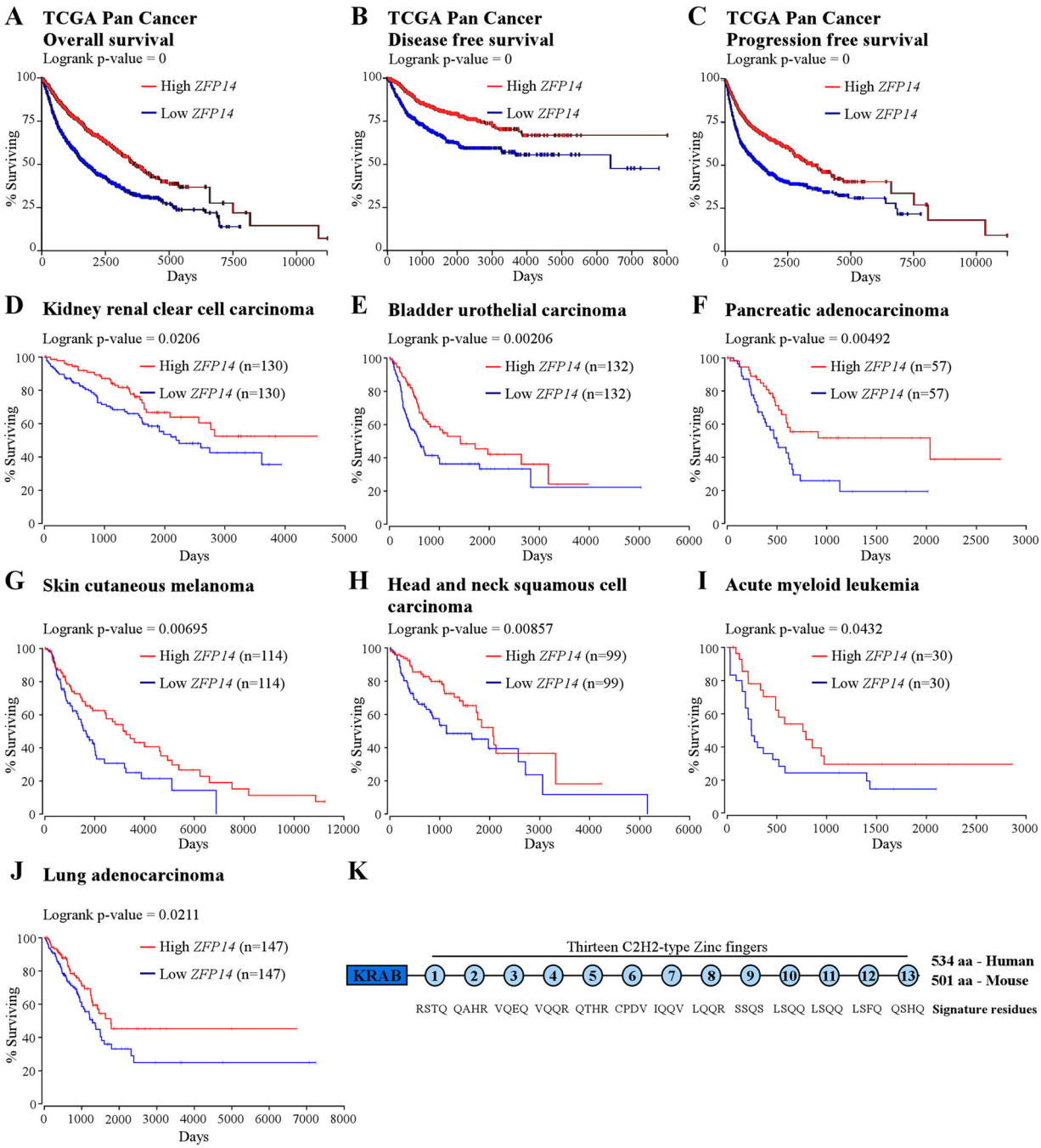

Fig. 1.

Low levels of *ZFP14* correlate with poor prognosis in human cancer patients.

(A-C) Kaplan-Meier survival curves showing low *ZFP14* expression correlating with poor overall survival (A), poor disease-free survival (B) and poor progression-free survival (C) in human cancer patients from TCGA pan-cancer database. The survival curves were created using the UCSC Xena browser.

(D-J) Kaplan-Meier survival analysis reveals that low *ZFP14* mRNA expression correlates with shorter patient survival in 8 types of tumors from TCGA database. The survival curves were created using the OncoLnc tool (http://www.oncolnc.org/).

(K) The KRAB domain and the C2H2 zinc fingers of human and mouse ZFP14 are depicted in the illustration. Also shown are the signature variable residues present at positions −1, +2, +3 and +6 in each zinc finger and are conserved between mouse and human ZFP14.

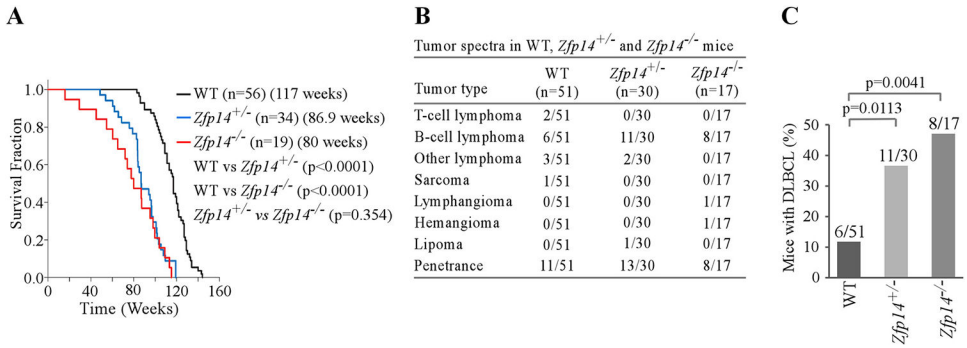

Tumor type	WT (n=51)	*Zfp14*$^{+/-}$ (n=30)	*Zfp14*$^{-/-}$ (n=17)
T-cell lymphoma	2/51	0/30	0/17
B-cell lymphoma	6/51	11/30	8/17
Other lymphoma	3/51	2/30	0/17
Sarcoma	1/51	0/30	0/17
Lymphangioma	0/51	0/30	1/17
Hemangioma	0/51	0/30	1/17
Lipoma	0/51	1/30	0/17
Penetrance	11/51	13/30	8/17

Fig. 2.

Zfp14$^{-/-}$ and *Zfp14*$^{+/-}$ mice have a shorter lifespan and are prone to spontaneous tumors.

(A) Kaplan-Meier survival curve for WT, *Zfp14*$^{+/-}$, and *Zfp14*$^{-/-}$ mice.

(B) Tumor spectra and penetrance in WT, *Zfp14*$^{+/-}$, and *Zfp14*$^{-/-}$ mice.

(C) The numbers and percentages of WT, *Zfp14*$^{+/-}$, and *Zfp14*$^{-/-}$ mice with DLBCL.

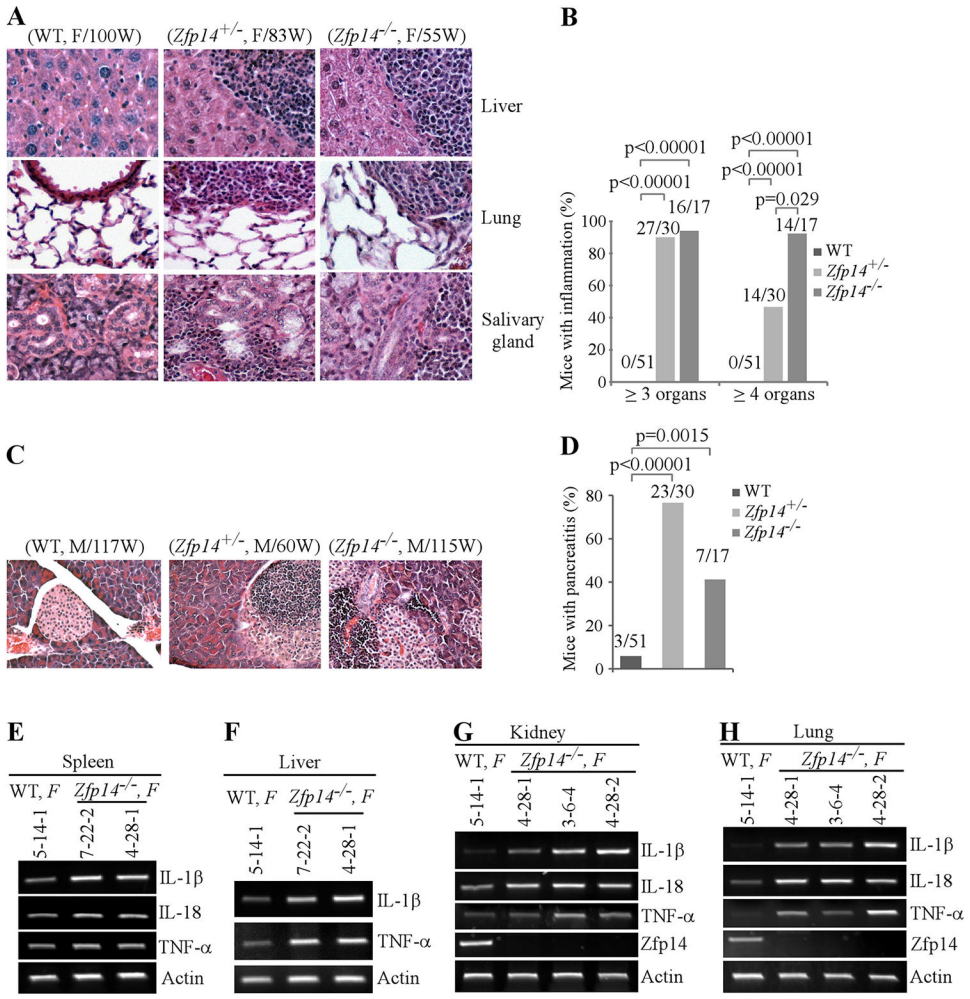

Fig. 3.

Zfp14-deficient mice are susceptible to inflammation and pancreatitis.

(A, C) Representative images of hematoxylin and eosin (H&E)-stained WT, *Zfp14*$^{+/-}$, and *Zfp14*$^{-/-}$ liver, lung and salivary gland showing inflammation (A) or pancreatitis (C).

(B, D) The numbers and percentages of WT, *Zfp14*$^{+/-}$, and *Zfp14*$^{-/-}$ mice with inflammation in >3 or >4 organs (B) or pancreatitis (D).

(E-F) The levels of various inflammatory cytokine mRNAs were quantified by RT-PCR in spleen (E), liver (F), kidney (G) or lung (H) of gender-matched WT and *Zfp14*$^{-/-}$ mice.

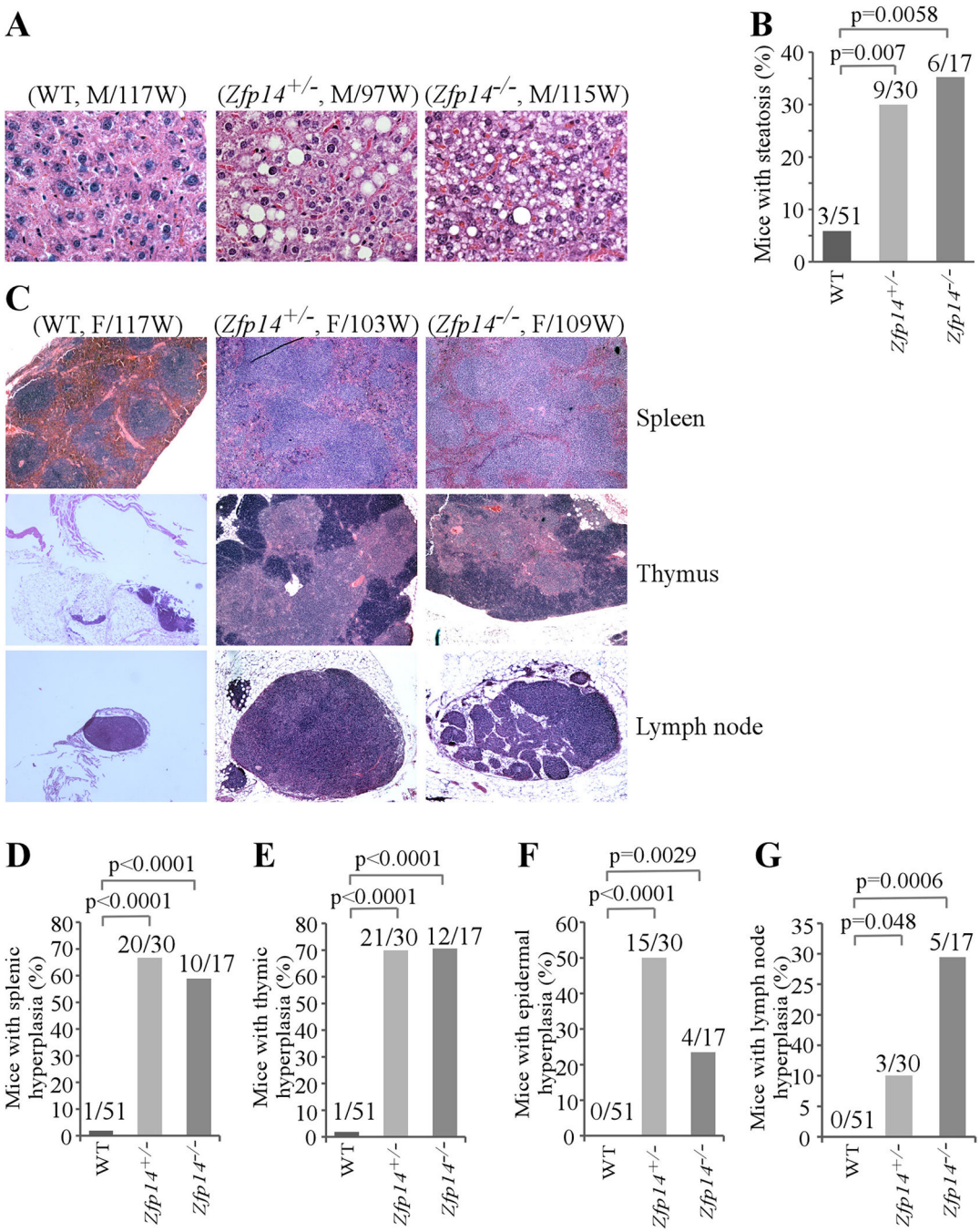

Fig. 4.

Zfp14-deficient mice are susceptible to liver steatosis and hyperplasia in multiple organs.

(A) Representative images of hematoxylin and eosin (H&E)-stained WT, *Zfp14*$^{+/-}$, and *Zfp14*$^{-/-}$ livers showing steatosis in *Zfp14*-deficient mice.

(B) The numbers and percentages of WT, *Zfp14*$^{+/-}$, and *Zfp14*$^{-/-}$ mice with liver steatosis.

(C) Representative images of hematoxylin and eosin (H&E)-stained WT, *Zfp14*$^{+/-}$, and *Zfp14*$^{-/-}$ spleen, thymus and lymph nodes showing hyperplasia in *Zfp14*-deficient mice.

(D-G) The numbers and percentages of WT, *Zfp14*$^{+/-}$, and *Zfp14*$^{-/-}$ mice with hyperplasia in spleen (D), thymus (E), skin (F) or lymph node (G).

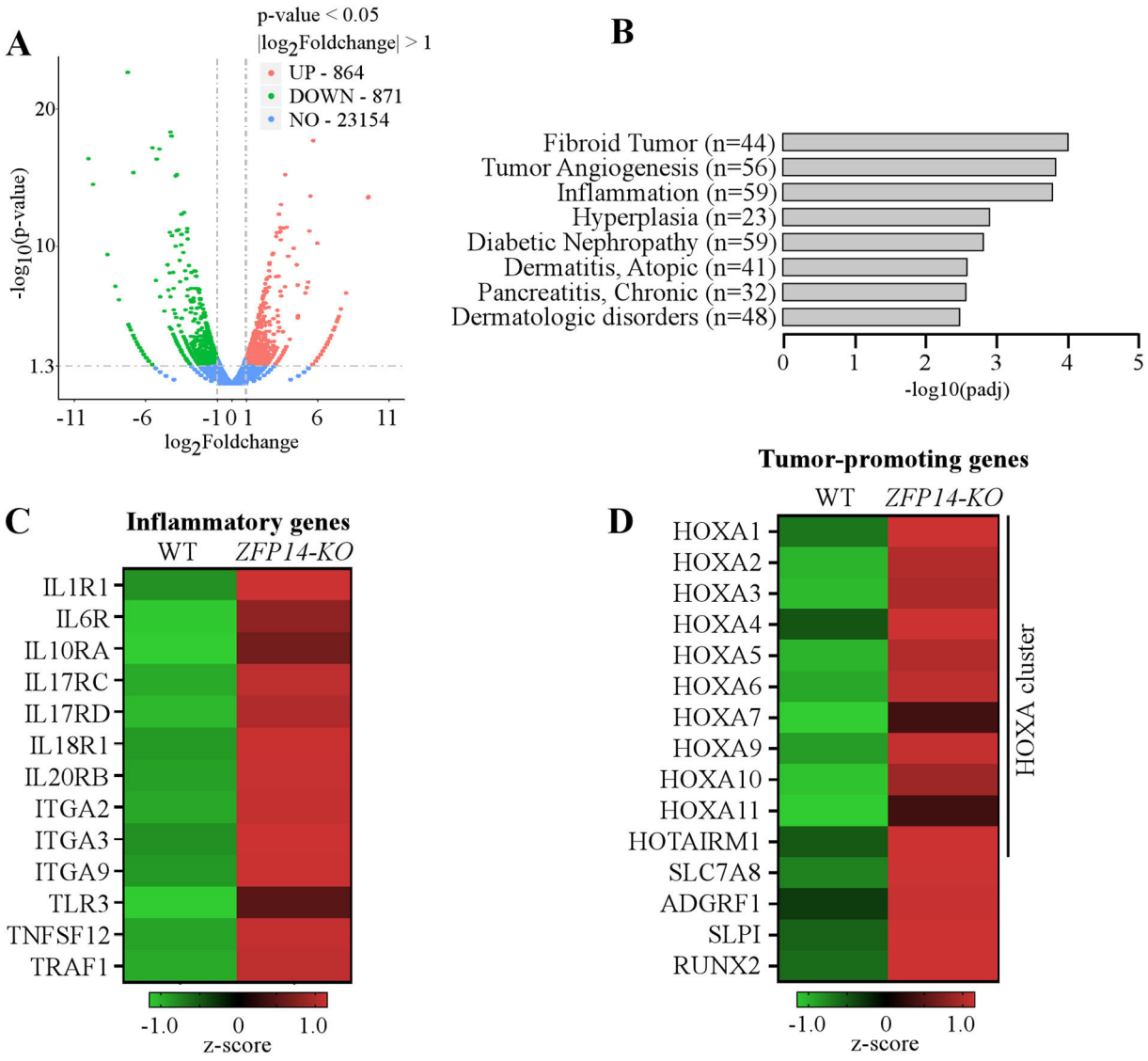

Fig. 5.

ZFP14-KO leads to increased expression of inflammatory and tumor-promoting genes.

(A) Volcano plot showing genes differentially regulated by ZFP14. The X-axis indicates fold-change and the Y-axis *p*-value.

(B) Gene-set enrichment analysis was performed to determine pathways differentially regulated by ZFP14.

(C, D) Heat map of inflammation-related genes (C) and tumor-promoting genes (D), and their differential expression in isogenic control and *ZFP14-KO* HCT116 cells.

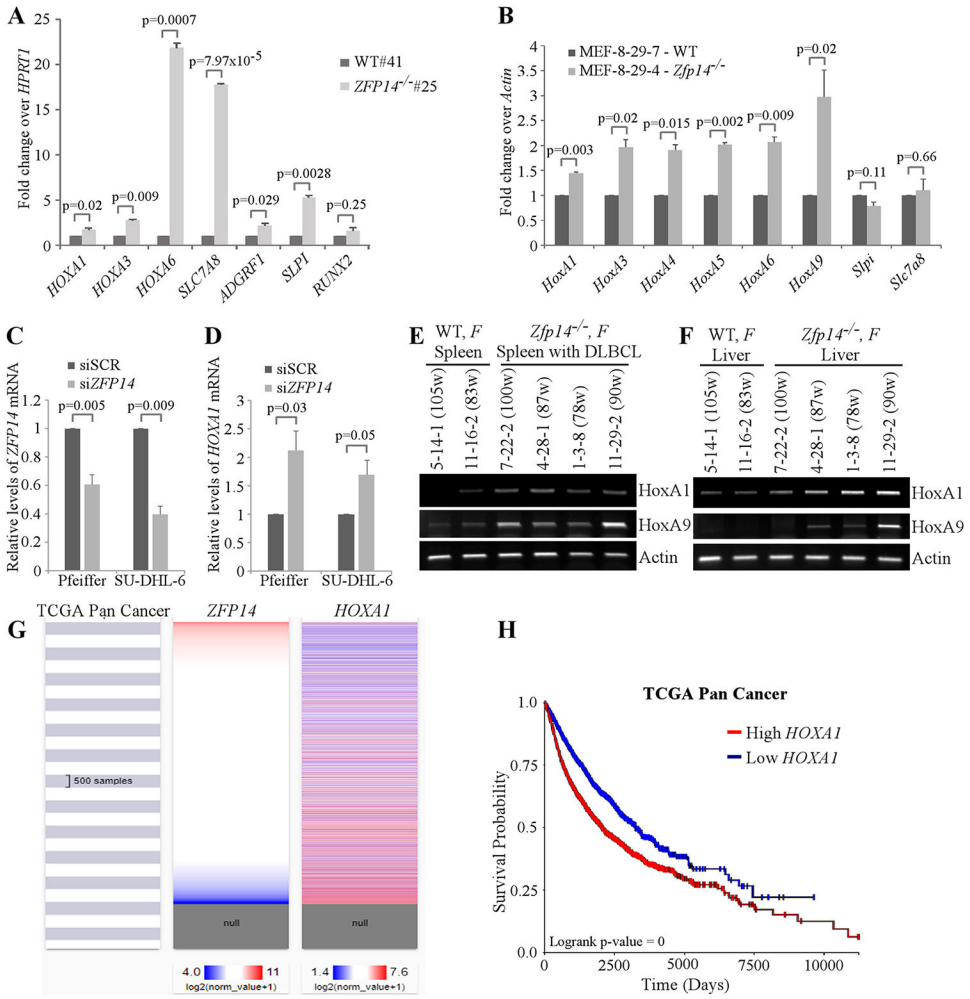

Fig. 6.

ZFP14 modulates tumorigenesis by regulating the expression of *HOXA* gene cluster in humans and mice.

(A) qRT-PCR confirmation of some ZFP14 regulated genes from RNA-seq in isogenic control and *ZFP14*-KO HCT116 cells.

(B) qRT-PCR was performed in WT and *Zfp14*$^{-/-}$ MEFs to confirm the regulation of some of the significantly regulated ZFP14 target genes from human cells.

(C-D) Pfeiffer and SUDHL6 cells were electroporated with scramble or *ZFP14* siRNA and the levels of *ZFP14* (C) and *HOXA1* (D) mRNAs were measured by qRT-PCR.

(E-F) The levels of *HoxA1* and *HoxA9* mRNA were quantified by RT-PCR in spleen (E) or liver (F) of gender-matched WT and *Zfp14*$^{-/-}$ mice.

(G) The inverse correlation of *ZFP14* expression with *HOXA1* gene expression in TCGA pan-cancer database using the UCSC Xena browser.

(H) Kaplan-Meier survival curve showing higher *HOXA1* expression correlating with poor prognosis in human cancer patients.